Journal of Chromatography A, 1218 (2011) 1983–1987

Contents lists available at ScienceDirect

Journal of Chromatography A

journal homepage: www.elsevier.com/locate/chroma

Short communication

A microfabricated graphitic carbon column for high performance liquid chromatography

D.A. Barrow[a,*], O.K. Castell[a,1], N. Sykes[a,2], P. Myers[b], H. Ritchie[c]

[a] Cardiff School of Engineering, Cardiff University, 1-5 The Parade, Cardiff CF24 3AA, UK
[b] Department of Chemistry, Liverpool University, Crown Street, Liverpool L69 7ZD, UK
[c] ThermoFisher Scientific Ltd., Tudor Road, Runcorn WA7 1TA, UK

ARTICLE INFO

Article history:
Available online 9 December 2010

Keywords:
Micropillars
Graphitic carbon
HPLC
Chromatography
Chip
Microfluidics
Femtosecond laser

ABSTRACT

We report the first development of a novel, planar, microfluidic, graphitic carbon separations column utilizing an array of graphitic micropillars of diamond cross-section as the chromatographic stationary phase. 795 nm femtosecond laser ablation was employed to subtractively machine fluidic architectures and a micropillared array in a planar, graphitic substrate as a monolithic structure. A sample injector was integrated on-chip, together with fluid-flow distribution architectures to minimize band-broadening and ensure sample equi-distribution across the micro-pillared column width. The separations chip was interfaced directly to the ESI probe of a Thermofisher Surveyor mass spectrometer, enabling the detection of test-mixture analytes following their differential retention on the micro-pillared graphitic column, thus demonstrating the exciting potential of this novel separations format. Importantly, unlike porous, graphitic microspheres, the temperature and pressure resilience of the microfluidic device potentially enables use in subcritical H_2O chromatography.

1. Introduction

Graphitic carbon has been explored as a stationary phase in chromatography since the 1970s because it extends the diversity of analytes that may be examined, widens the range of mobile phases employed and enables separations over a greater range of pH [1,2]. Graphitic carbon has taken several forms including (i) pyrolytic carbon coatings on graphitized carbon black or silica particles [3], (ii) porous glassy carbon [1], (iii) porous graphitic carbon [4], and (iv) colloid-imprinted carbon [5]. Porous graphitic carbon became the most popular form due to its better chromatographic performance and excellent mechanical stability. It is marketed as Hypercarb® by Thermofisher corporation, BTR Carbon® by Biotech Research, and TSK-gel Carbon-500® by Tosoh Corporation. As a stationary phase material, graphite has enabled opportunities to enhance separation efficiency due partly to the homogeneity of graphitic, isotropic, crystalline surfaces which affords high reproducibility and total pH stability. Two recent reviews by Periera [6] and West et al. [7] provide an extensive analysis of porous graphitic carbon for use in chromatography. It has been previously reported [7] that Agilent and SGE have both introduced HPLC-chips using graphitized carbon packings, but questions persist over chip-to-chip reproducibility.

Generally, separations columns of packed, porous, particulate material afford significant analyte capacity. However, separation efficiency is sub-optimal [8], due to inhomogeneities in the stationary-phase packing and axial analyte diffusion [9]. Due to advances in chip-based microfluidics [10] and micropackaging [11] which, in turn, have given rise to diverse, novel, separations processes [12,13], these inhomogeneities can be addressed through the production of highly ordered, micromachined, pillared arrays [14,15], as predicted by computational fluid dynamics studies of such [16]. Most previous studies have used deep-reactive-ion-etching of silicon to produce high aspect-ratio pillars of various geometries [17], but this process cannot be practiced on graphite.

In order to manufacture similar structures in graphite we have provisionally explored the use of 795 nm femtosecond laser ablation to subtractively micromachine a micropillared column in a planar, graphitic substrate as a single, monolithic structure. A sample injector was integrated on-chip, together with fluid-flow distribution architectures to minimize band broadening and ensure sample equi-distribution across the micro-pillared column width.

2. Materials and methods

2.1. Graphitic carbon substrates

Porous, ultrafine grain, isotropic graphite (EC-17 grade) impregnated with phenol formaldehyde resin, with an average grain size of

* Corresponding author. Tel.: +44 0 2920875921; fax: +44 0 2920874716.
E-mail address: barrow@cf.ac.uk (D.A. Barrow).
[1] Now at Chemistry Research Laboratory, Oxford University, 12 Mansfield Road, Oxford OX1 3TA, UK.
[2] Now at Micronanics Ltd., Harwell Campus, Didcot OX11 0QX, UK.

0021-9673/$ – see front matter © 2010 Elsevier B.V. All rights reserved.
doi:10.1016/j.chroma.2010.11.086

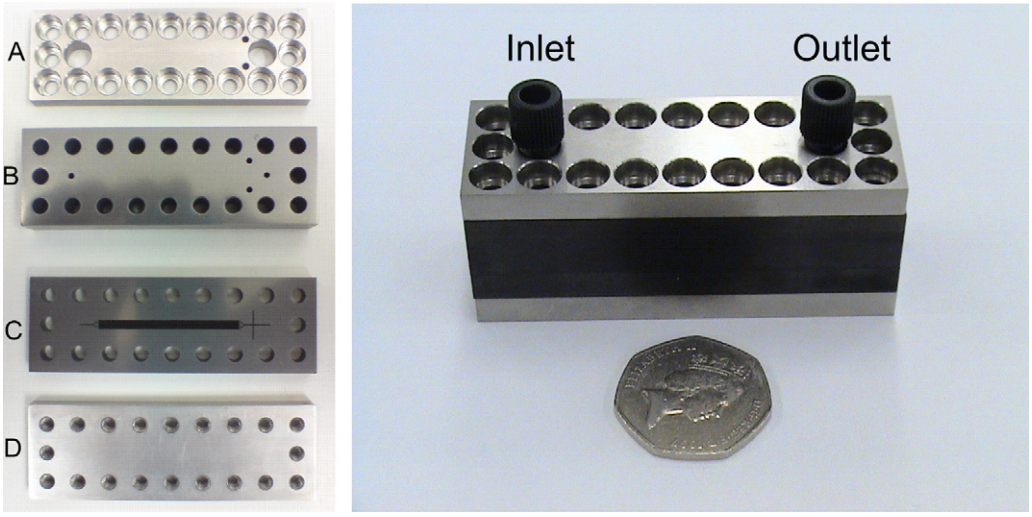

Fig. 1. Left: Image of component layers which constitute the assembled separations column, comprising (A) top stainless steel compression plate, (B) interface/capping layer of graphite, (C) substrate layer of graphite (with integrated column, fluid distributor and injector), and (D) bottom stainless steel compression plate. Right: Image of the stacked graphitic column assembly; this shows an initial version which did not incorporate an integrated sample injector.

2 μm, was obtained from GraphiteStore.com Inc. (Buffalo Grove IL, USA). This was machined to a rectangular format (76 mm × 25 mm) using standard mechanical workshop milling machines. 6 mm thick substrate layers and 12 mm thick fluidic interfacing layers were produced (Fig. 1).

2.2. Device manufacture and assembly

M6 tap (8 mm depth) and 1/16″ drill holes were machined in the graphitic fluidic interfacing layer and served as inlet/outlet ports (5 cm apart, each 2.5 cm from substrate centre point). In addition, 1/16″ drill holes were made to house PEEK capillaries which served to interface with the sample phase injector inlet/outlet ports. Both top and bottom graphitic substrate layers were drilled with 20 through-holes, equidistantly spaced around the substrate perimeter, to accommodate M4 bolts of the device compression system (Fig. 1). A 76 mm × 25 mm × 6 mm stainless steel compression manifold was prepared and drilled and threaded to accept M4 bolts to enable device compression. Additional holes were drilled in the upper portion of the manifold to enable fluidic interfacing with the inlets and outlets of the graphitic device.

Graphite substrates were manually polished using cerium oxide optical polishing powder and a water wetted, fine (1200 grit) polishing pad. Hand pressure was manually applied to the graphitic substrate which was moved back and forth along the long axis of the substrate. The material was washed and dried at intervals of 2–3 min, with water and optical polishing powder re-applied to the polishing pad. A Computer-Aided-Design (CAD) file in dfx format was generated to control the movement of the laser workstation stage (on which the graphite was located) in relation to the fixed position laser beam (Fig. 2). The CAD file instructed single sweeps of the laser which would subtractively remove graphite and thus create gaps in between the remaining pillars. The CAD file was designed to create an array of ~0.53 million micropillars over a length of 37 mm and 2.3 mm width. Half-diamond, pillared features at the column edge were designed to reduce band broadening by minimizing column inhomogeneities at the column perimeter. At each end of the micropillared column, fluid distributors (based on serial bifurcating ducts) were designed such that fluid would interface to the column with minimal band broadening. This would otherwise be likely to occur since the column took on an essentially wide, but shallow format, that needed to be interfaced with circular cross-section PEEK tubing to pumps and the mass-spectrometer electrospray interface probe (ESI probe). The fluid distributor required considerable removal of graphite and therefore multiple, parallel passes of the laser beam were designed into the CAD file. Additionally, as the number of bifurcations progressively reduced within the distributors, the duct depth correspondingly increased to convert the wide and shallow format into one more similar to the circular cross-section of the PEEK tubing connectors.

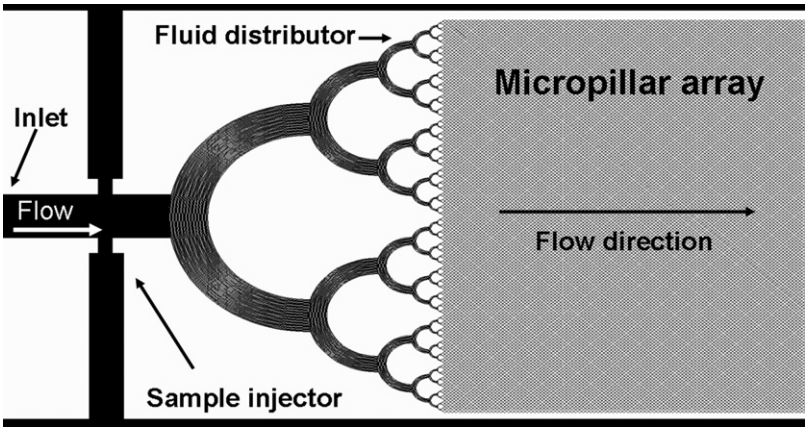

Fig. 2. CAD layout of graphitic separations device showing fluid distributor, injector and proximal end of pillared column.

There have been only a few studies on the femtosecond laser ablation of graphite, mainly looking at the dynamics of the actual ablation process [18]. It has been shown that ablation debris forms carbon nanoflakes [19] and carbon nanotubes. Our own early trials, where we compared excimer (193 nm and 157 nm) and femtosecond laser ablation, showed that fine structures could be readily micromachined in graphite with the femtoseccond laser. Accordingly, the polished and dried graphitic substrate was subtractively ablated with a 1.5 W Thales Bright femtosecond laser (790 nm wavelength), power 0.4 W, 120 fs pulse-width, feed-rate 100 mm/min, triplet lens, single pass) to produce a separations column 3.7 cm in length and 2.3 mm in width. A nanolitre volume, x-junction, sample injector was integrated on the chip.

2.3. Design of fluidic architecture

A separations column consisting of 5.3×10^5 free-standing pillars ($12.7\,\mu m \times 12.7\,\mu m \times 14\,\mu m$ depth) was achieved by laser ablation of multiple, parallel and perpendicularly intersecting ducts machined at an angle of 45° from the separation column's long axis. A Mathcad 11.0 (mathsoft) fluid dynamics model of the column architecture calculated that a desired flow rate of 0.001 ml min^{-1}, achieved through a pressure drop of 0.2 MPa (30 psi), would be required to realize a comparable transit time to that of a macroscale (3 mm × 50 mm) Hypercarb test column at the employed test flow-rate of 0.32 ml min^{-1}.

2.4. Integration with Thermofisher HPLC-MS equipment

Injections were conducted utilising a pressure-based delivery method, by utilising on/off tap valves either side of the injector inlet and outlet. 0.005″ ID, 1/16″ OD PEEK tubing interfaced the graphitic device at the mobile phase inlet and outlet and sample phase injector inlet. 0.010″ ID, 1/16″ OD PEEK tubing interfaced the sample phase injector outlet to ensure preferential flow across the sample injector during the sample injection procedure.

MS integration was achieved with a custom, coaxial-flow make-up to ensure sufficient liquid delivery to the Thermofisher MS ESI probe, thus enabling efficient eluent electrospray ionization. A coaxial make-up assembly assembled from a Tefzel® T-junction with a 0.02″ through-hole interfaced with 1/16″ OD tubing. A fused silica capillary (125 μm OD 50 μm ID) was passed through the T-junction through-hole, with the 0.005″ ID, 1/16″ OD PEEK tubing of the graphitic device outlet acting as a tight sleeve for the fused silica capillary. Thus, eluent flow from the chip was directed into the fused silica capillary, which, after passing through the central region of the T-junction union, terminated centrally within 1/16″ OD 0.5 mm ID FEP tubing. This FEP tubing carried the make-up flow (methanol + 1% acetic acid 0.2 ml min^{-1}), originating from an independent HPLC pump, and delivered fluid-flow to the perpendicular input of the T-junction.

2.5. Test mixtures

As a first demonstration to evaluate this graphitic HPLC chip, acrylamide and hydrocortisone were used as test analytes. These would exhibit significant differential retention, and could be detected under the same ionization mode conditions.

3. Results and discussion

3.1. Device construction

The use of the femtosecond laser in removing graphite showed that material ablation was achievable, even at low power settings (Fig. 3). However, the Gaussian beam profile used left a tapered groove between pillars, which functionally would enable an unequal fluid flow velocity distribution in the *z*-axis plane of the column, and contribute to band broadening. The widest section of the groove at the top was too large for significant chromatographic purposes, whilst that further down the groove reached almost ideal sub-micron dimensions.

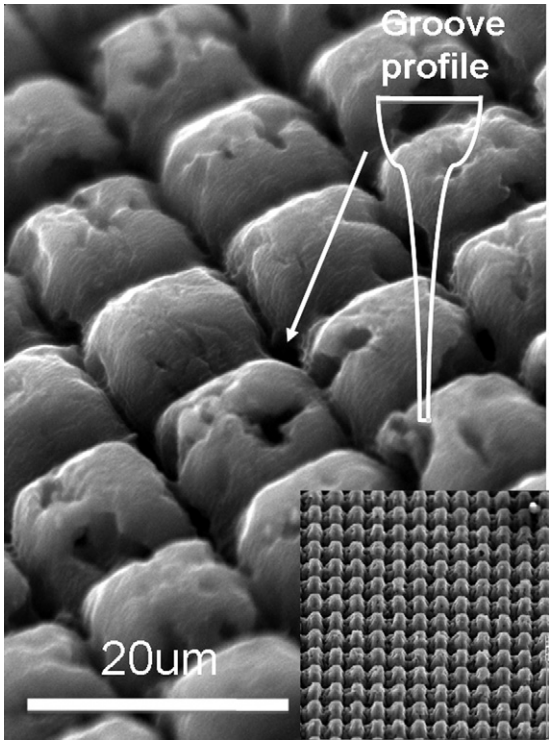

Fig. 3. Detailed image of pillars and groove profile showing tapered interpillar gap left from ablation by the femtosecond laser.

Most preferably, an equidistant, sub-micron groove should be attained, to be comparable with conventional packed media columns. Also, the height of the pillars was limited to ~14 μm, whereas, a height of 10 times this measure is preferred, not least, to increase the column capacity and surface area.

3.2. Device operation

Using a Rheos 2000 pump, mobile phase (75% H_2O/25% MeOH + 0.25% acetic acid) was delivered at 0.001 ml min^{-1} with a backpressure of 35 psi. Prior to each injection, the flow rate of mobile phase was increased to 0.005–0.02 ml min^{-1} for several minutes, before reducing the pumping flow rate to 0.001 ml min^{-1}. As the residual back pressure fell from 500 psi to 35 psi, manual injections were made at back pressures of ~140 psi. A reproducible method of sample injection was developed which involved the rapid (1–3 s) addition of a small volume of sample phase flow (added via the sample injector inlet), to the continuously flowing mobile phase flowing through the pillared column, thus allowing a small addition of the analyte sample. The injection was made by physical compression of the syringe driver manifold at the time of opening the sample phase inlet valve. Using this procedure, the quantity of sample injected was unknown, although the measured response at the MS detector (Fig. 4) was found to be reproducible on repeat injections (Fig. 5), and varying the time that the inlet valve remained open could modulate the injection size. The sample phase injected was, however, much greater than the injector x-junction, intersection volume (1.9 nl), as evidenced by flooding.

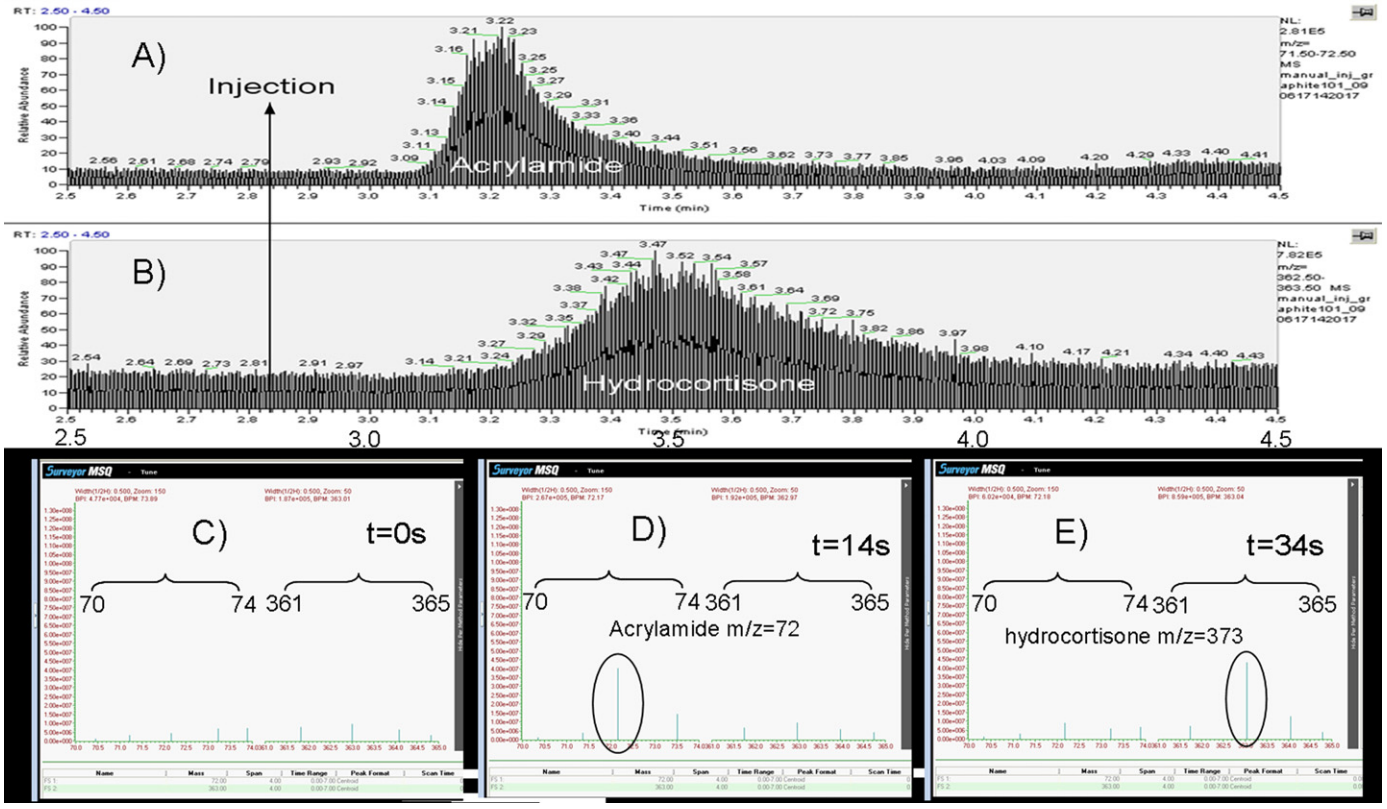

Fig. 4. Acrylamide (A) and hydrocortisone (B) differential retention on laser machined microfluidic graphitic column. Mobile phase H_2O/MeOH (75/25) + 0.25% acetic acid, mobile phase delivery pressure 194 psi. Post-chip electrospray make-up of MeOH + 1% acetic acid (0.2 ml min^{-1}). Sample phase acrylamide (0.1 ml min^{-1}) and hydrocortisone (0.1 ml min^{-1}) in H_2O/MeOH (75/25) + 1% acetic acid. Differential retention of acrylamide and hydrocortisone on competitive injection of a combined mixture of the two analytes. ESI mass spectra viewed at each of the specific mass ranges for acrylamide (71.5–72.5 *m*/*z*) and hydrocortisone (362.5–363.5 *m*/*z*) at (C) *t* = 0 s, (D) *t* = 14 s, and (E) *t* = 34 s.

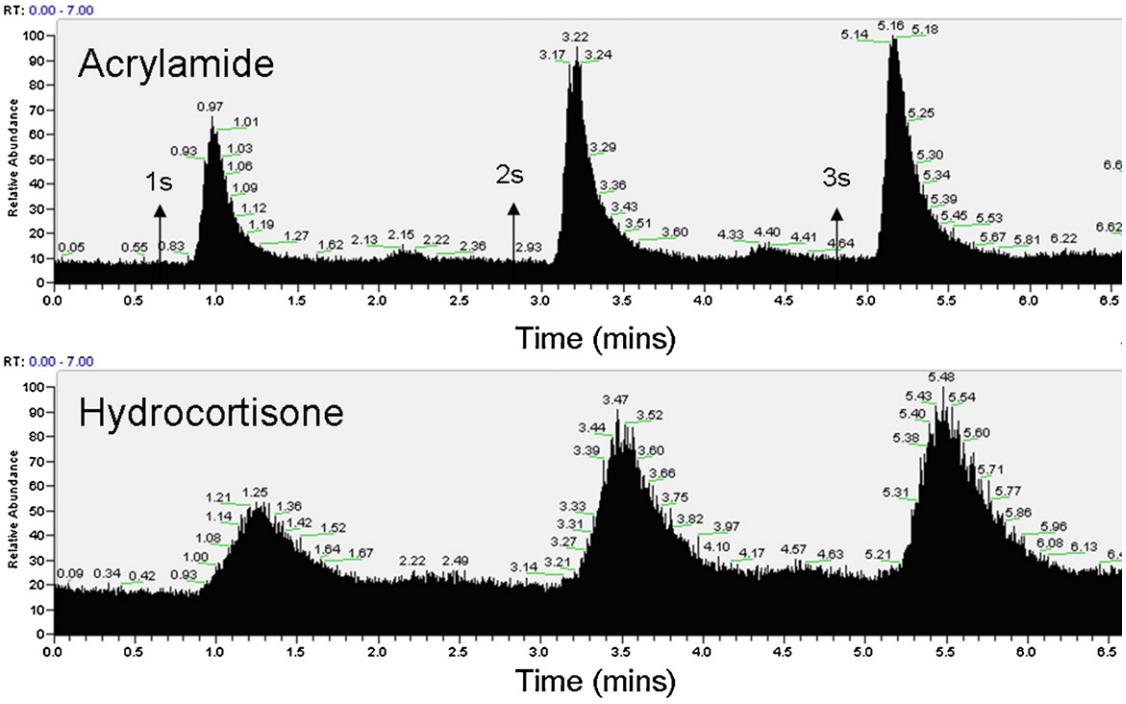

Fig. 5. Three repeat injections of the acrylamide/hydrocortisone test mix. In each successive injection the injector valve was opened for an increasing duration (~1, ~2, and ~3 s, respectively), demonstrating the flooding of the sample injector x-junction. This results in a larger than desired sample injection volume and therefore loss of temporal resolution in the separation as the injection slug volume becomes increasingly significant compared to the low volume of the separations column itself. It is proposed that a dramatically improved separation may be achieved on development and integration of a finely controlled, on-chip, sample phase injector. Arrows mark injection events.

3.3. Detection

The device was connected directly to a Thermofisher Surveyor ESI interface for mass-spectrometry detection, using methanol + 1% acetic acid flow make-up. Mass spectra data were acquired in positive ion mode, with mass ranges of 71.5–72.5 m/z (gain, 150) and 362.5–363.5 m/z (gain, 50) recorded simultaneously for acrylamide and hydrocortisone, respectively (scan time 0.08 s) with a needle voltage of 5KV, probe temperature of 519 °C and cone voltage of 55 °C. Analyte specific mass-range monitoring was employed due to the low total quantity of analyte in the post-make-up flow stream, resulting in significant noise in the total-ion-current recorded by the detector.

3.4. Further improvements

Although a significant difference in retention of the two eluting test species was demonstrated, 100% baseline resolution of the component peaks was not achieved under the evaluated test conditions. This was reasoned to be due to several contributing factors which may be significantly improved upon with further development, including (A) use of newly available ultraflow-rate gradient HPLC pumps, (B) an improved, sample injection process to reduce flooding, since the injected sample volume approached that of the column (0.38 μL), (C) use of a parallel fluidic exit, the elimination of void volumes and a reduction in the post-separation flow-distance to detector, (D) increased column capacity, and (E) use of on-chip, integrated, ultraviolet detection and/or ESI probe. Additionally, femtosecond laser machining of graphite with a Bessel beam would enable closer packing and higher aspect-ratio micropillars whilst mask-projection excimer laser would accelerate production time and improve sidewall verticality. Creating a micropillared device increased the surface area by 250 times compared to an open, tubular duct but needs increasing by a further few orders of magnitude. This could be done by electrochemical anodization [20,21] to induce porosity or through the growth of highly graphitized carbon nano-rods or carbon nanotubes from the micropillar surface [22]. Electrochemically modulated retention could also be enabled by the conductive nature of the graphite, as done with columns packed with porous graphitic spheres [23,24].

4. Conclusions

The differential retention of two analytes in a single, sample phase has been demonstrated using a laser-micromachined, graphitic, microfluidic device interfaced to a macro-scale mass spectrometer and traditional HPLC-style machinery. With future improvements implemented, the miniaturized graphitic separations platform showed promise for the future development of high-efficiency, rapid, chemical separations. The microfluidic device format enables <1 min run times with low reagent consumption and low requirement for analyte matrix volume, using highly ordered, pillared, stationary-phase structure and flow distribution architectures, improving the theoretical separation efficiency over traditional microsphere packed-bed columns. Ultimately, solid-state, microfluidic, graphitic, separations devices may be used at high temperatures and pressures to enable the use of subcritical, water chromatographic techniques. These could offer practical, safety and environmental advantages over traditional, organic, solvent orientated, separation methodologies. Towards this aim, the reported device has been demonstrated to withstand high-pressure flow without leakage (~350 psi), which may be further improved through the use of a polyamide imide bonding resin between substrate layers.

Acknowledgements

This work was undertaken at the UK metaFAB nanocentre facility with support from the UK government Technology Strategy Board, Thermofisher UK Ltd. and Nikon (UK) Ltd. Some of this work was done by Neil Sykes towards a MSc. in laser micromachining.

References

[1] M.T. Gilbert, J.H. Knox, B. Kaur, Chromatographia 16 (1982) 138.
[2] J.H. Knox, B. Kaur, G.R. Millward, J. Chromatogr. 352 (1986) 3.
[3] H. Colin, G. Guiochon, J. Chromatogr. 137 (1977) 19.
[4] J.H. Knox, K.K. Unger, H. Mueller, J. Liquid Chromatogr. 6 (1983) 1.
[5] Z. Li, M. Jaroniec, J. Am. Chem. Soc. 123 (2001) 9208.
[6] L. Pereira, J. Liquid Chromatogr. 31 (2008) 1687.
[7] C. West, C. Elfakir, M. Lafosse, J. Chromatogr. A 1217 (2010) 3201.
[8] J.H. Knox, J. Chromatogr. A 831 (1999) 3.
[9] J. Eijkel, Lab. Chip 7 (2007) 815.
[10] D.A. Barrow, S.E. Taylor, J.J. Cefai, Chem. Ind. Lond. 15 (1999) 591.
[11] T. Velten, H. Ruf, D. Barrow, N. Aspragathos, P. Lazarou, E. Jung, C. Khan Malek, M. Richter, J. Kruckow, M. Wackerle, IEEE Trans. Adv. Pack. 28 (2005) 533.
[12] O.K. Castell, C.J. Allender, D.A. Barrow, Lab. Chip 7 (2008) 1031.
[13] O.K. Castell, C.J. Allender, D.A. Barrow, Lab. Chip 8 (2009) 388.
[14] B. He, F. Regnier, J. Pharmaceut. Biomed. 17 (1998) 925.
[15] W.D. Malsche, D. Clicq, V. Verdoold, P. Gzil, G. Desmet, H. Gardeniers, Lab. Chip 7 (2007) 1705.
[16] J. De Smet, P. Gzil, N. Vervoort, G.V. Baron, G. Desmet, Anal. Chem. 76 (2004) 3716.
[17] W. Park, J. Kim, J.H.S.M. Cho, S.G. Yoon, S.J. Suh, D.H. Yoon, Surf. Coat. Technol. 171 (2003) 290.
[18] S. Amoruso, G. Ausanio, M. Vitiello, X. Wang, Appl. Phys. A: Mater. 81 (2005) 981.
[19] M. Lenner, A. Kaplan, Ch. Huchon, R.E. Palmer, Phys. Rev. B 79 (2009) 1.
[20] W.R. Matson, US Patent 6573106, 2003.
[21] V.A. Karavanskii, N.N. Melnik, T.N. Zavaritskaya, Phys. Status Solidi A 197 (2003) 192.
[22] A. Fonvernea, F. Ricoula, C. Demesmayb, C. Delattrea, A. Fournierc, J. Dijonc, F. Vineta, Sensor. Actuat. B: Chem. 129 (2008) 510.
[23] E. Ting, M.D. Porter, J. Electroanal. Chem. 180 (1998) 185.
[24] R. Saari-Nordhaus, L.M. Nair, R.M. Montgomery, J.M. Anderson Jr., J. Chromatogr. A 782 (1997) 60.